Super-resolution deep learning reconstruction at coronary computed tomography angiography to evaluate the coronary arteries and in-stent lumen: An initial experience

Makoto Orii (kori931@gmail.com)
Department of Radiology, Iwate Medical University
Misato Sone
Department of Radiology, Iwate Medical University
Takeshi Osaki
Department of Radiology, Iwate Medical University
Yuta Ueyama
Center for Radiological Science, Iwate Medical University
Takuya Chiba
Center for Radiological Science, Iwate Medical University
Tadashi Sasaki
Center for Radiological Science, Iwate Medical University
Kunihiro Yoshioka
Department of Radiology, Iwate Medical University

Research Article

Keywords: coronary computed tomography angiography, super-resolution deep learning reconstruction, model-based iterative reconstruction, signal-to-noise ratio, contrast-to-noise ratio

Posted Date: July 22nd, 2022

DOI: https://doi.org/10.21203/rs.3.rs-1875541/v1

Abstract

The present study aimed to compare the image quality of the coronary arteries and in-stent lumen between super-resolution deep learning reconstruction (SR-DLR) and model-based iterative reconstruction (MBIR). We prospectively enrolled 50 patients (median age, 68 years; interquartile range [IQR], 59–74 years; 34 men) who underwent coronary computed tomography angiography (CCTA) using a 320-detector row CT scanner between January and April 2022. The image noise in the ascending aorta, left atrium, and septal wall of the ventricle was measured, and the signal-to-noise ratio (SNR) and contrast-to-noise ratio (CNR) in the proximal coronary arteries were calculated. Of the ten stents, stent strut thickness and luminal diameter were quantitatively evaluated. The image noise on SR-DLR was significantly lower than that on MBIR (median 22.1 HU; IQR, 19.1–24.5 HU vs. 27.4 HU; IQR, 24.1–31.1 HU, $p < 0.01$), whereas the SNR (median 16.3; IQR, 12.0–22.0 vs. 13.9; IQR, 9.8–19.2, $p = 0.03$) and CNR (median 25.2; IQR, 16.9–30.8 vs. 19.5; IQR, 14.5–23.7, $p < 0.01$) on SR-DLR were significantly higher than that on MBIR. Stent struts were significantly thinner (median, 0.66 mm; IQR, 0.61–0.72 mm vs. 0.80 mm; IQR, 0.68–0.86 mm, $p < 0.01$) and in-stent lumens were significantly larger (median, 1.82 mm; IQR, 1.57-1.95 mm vs. 1.34 mm; IQR, 1.26–1.60 mm, $p < 0.01$) on SR-DLR than on MBIR. This study's initial experience with SR-DLR improves the image quality of the coronary arteries and in-stent lumen at CCTA compared with conventional MBIR.

Introduction

Coronary computed tomography angiography (CCTA) is a robust noninvasive imaging technique with high spatial and temporal resolutions. Its diagnostic accuracy is high for the exclusion of coronary artery disease; however, some factors such as high image noise, insufficient vessel enhancement, and blooming- and beam-hardening artifacts may hamper the precise evaluation of vessel stenosis and in-stent lumen [1-3].

Recent CCTA developments with an ultrahigh spatial resolution computed tomography (UHRCT) of 0.25 mm × 128 or 160-row detector and model-based iterative reconstruction (MBIR) have overcome the limitations of the current CT spatial resolution. Several studies have reported higher diagnostic accuracy to detect significant stenosis with severely elevated calcium scores and in-stent patency with a diameter of ≥2.5 mm; however, the use of UHRCT is limited for patients with higher heart rate and weight and those with arrhythmia [4-6].

Recently, a super-resolution deep learning reconstruction (SR-DLR) algorithm trained using data acquired on the commercially available UHRCT system is available for the whole-heart, single-rotation cardiac coverage on a 320-detector row CT scanner [7]. SR-DLR has the potential to accurately diagnose coronary arteries and stent structures by combining exceptional spatial resolution, noise reduction, and single rotation coverage. However, no studies have reported data on the potential value of SR-DLR at CCTA in the clinical setting. Thus, this study aimed to compare the image quality of the coronary arteries and in-stent lumen during CCTA reconstructed using SR-DLR and MBIR.

Material And Methods

Study population and design

Fifty consecutive patients who underwent CCTA for suspected or known coronary artery disease between January and April 2022 were prospectively enrolled at Iwate Medical University Hospital. Our exclusion criteria were renal insufficiency (estimated glomerular filtration rate < 30 mL/min per 1.73 m^2), contrast agent allergy, history of bypass grafting, and potential pregnancy. Written informed consent was obtained from all participants, as approved by the institution's human research committee.

CT scanning

CT scans were performed using a 320-detector row CT scanner (Aquilion ONE PRISM Edition, Canon Medical Systems, Otawara, Japan). All patients were administered nitroglycerin. Patients with a heart rate of 65 bpm were administered oral beta-blockers 60 min before the CCTA scan based on the Society of Cardiovascular Computed Tomography guidelines [8,9].

Coronary calcium scoring was performed using a prospective electrocardiogram (ECG) gating axial scan at a 75% RR interval, with 120 kV tube voltage and a 300-mA tube current. We delivered 25.9 mgI/kg/s of nonionic contrast material (iopamidol [Iopamiron 370, Bayer, Osaka, Japan]) at a 10-s fixed duration, followed by a 35-mL saline flush administered using a 20-G intravenous catheter. The scan parameters were collimation of 320 × 0.5 mm; rotation time, 0.275 s; z-coverage, 120–160 mm; tube voltage, 100 or 120 kV; and tube current, 180–750 mA. Prospective ECG gating scan with an acquisition window of 35%–80% or 65%–80% of the RR interval was used for patients with a heart rate of >65 or ≤65 bpm, respectively. Retrospective ECG gating scan was used for patients with arrhythmia or those who could not sufficiently hold their breath. Experienced cardiovascular CT technologists determined the optimal stationary cardiac phase with minimum motion-free datasets. The dose length product was recorded for each participant, and the corresponding effective radiation dose was calculated using a standard conversion factor of 0.014 mSv/mGy cm for chest CT [10]. Axial images were reconstructed with 0.5-mm slice thickness and reconstruction interval. The image reconstruction field of view and the matrix size were 160–200 mm and 512 × 512, respectively. All images were reconstructed using the SR-DLR (PIQE) and MBIR algorithm (FIRST, Canon Medical Systems Corp.).

Image interpretation

The image datasets were transferred to an off-line workstation, processed using commercially available software (Ziostation2, Ziosoft Inc., Tokyo, Japan) and two radiologists (M.O. and K.Y.) with 5 and 25 years of experience, respectively, in cardiovascular imaging performed all measurements. The readers were blinded to the clinical information and reconstruction method. In case of data analysis disagreed, a final decision was reached by consensus. The degree of coronary stenosis was graded as minimal (<25%), mild (25%–49%), moderate (50%–69%), and severe (70%–99%) [11].

The overall image quality of each coronary artery segment was rated based on a four-point rating score for each coronary artery segment (4, excellent [minimal or no noise-related blurring and diagnostic information sufficient); 3, good [some noise-related blurring and diagnostic information acceptable]; 2, fair [marked noise-related blurring and diagnostic information limited]; and 1, poor [blurry and diagnostic information impaired]) [12].

For SR-DLR and MBIR images, the image noise was recorded as the standard deviation (SD) of the attenuation value in a circular region of interest (ROI) placed in the ascending aorta, left atrium, and septal wall of the ventricle. Then, signal-to-noise ratio (SNR) was calculated as signal/noise in the proximal right coronary artery and left main trunk [6]. The contrast-to-noise ratio (CNR) was calculated as follows: (mean vessel lumen signal − mean perivascular fat signal)/image noise in the ascending aorta [13,14]. ROI measurements were performed by two radiologists on axial images, carefully preventing calcifications, plaques, and stenosis.

In-stent lumen assessability and quantitative stent analysis

Stents were considered assessable with the absence of partial volume effects by stent struts, beam hardening, motion artifacts, calcification, or low CNR and when the lumen within the stent was clearly visible [4,15]. Fig 1 shows the calculation methods of lumen visibility measurements using the average attenuation profile in the axial plane [4,15]. First, the stent proximal and distal edges on the curved planar reformation (CPR) image were determined, with the first, second, and third quartiles as calculated points. Second, after determining the center of the stent on the cross-sectional image (Fig 1a and b), attenuation profiles were calculated, and the full width at half maximum of the lumen (FWHM-lumen) and full width at half maximum of the strut (FWHM-stent) were measured (Fig 1c and d).

Statistical analysis

Statistical analyses were performed using IBM® SPSS® 28.0.1 (IBM Corporation., Armonk, NY, USA). Continuous measurements are expressed as mean ± SD for normally distributed variables or median (interquartile range [IQR], 25th–75th percentile) for nonparametric data and compared using Student's t-test or Mann–Whitney U-test as appropriate. Categorical variables are expressed as numbers and percentages. p-value of < 0.05 was considered statistically significant. The interobserver agreement between two radiologists regarding the qualitative evaluation was evaluated using the Cohen kappa κ coefficient. A κ value of more than 0.81 corresponded to excellent interobserver agreement, while values of 0.61–0.80 corresponded to good agreement.

Results

Table 1 lists the baseline clinical characteristics of 50 patients (median age, 68 (IQR, 59–74) years; 34 men). Seven patients had prior stent placement (a total of 10 stents). The median body mass index of patients was 24 (IQR, 22–26) kg/m^2; their median heart rate during scanning was 56 (IQR, 51–63) bpm.

Of the 50 patients, 44 underwent imaging with prospective ECG gating, and the other six were imaged with retrospective gating due to arrhythmia or insufficient breath-hold. In patients without stents, the median calcium score was 3 (IQR, 0–127). The median effective radiation dose was 0.7 (IQR, 0.6–1.6) mSv.

Comparison of SR-DLR and MBIR

Table 2 displays the reconstruction time, image noise, SNR, CNR, and visual evaluation of the coronary arteries between SR-DLR and MBIR. The reconstruction time was significantly shorter on SR-DLR than on MBIR (median, 97 s; IQR, 88–103 s vs. 172 s; IQR, 161–185 s, $p < 0.01$). The image noise was significantly lower on SR-DLR than that on MBIR (median 22.1 HU; IQR, 19.1–24.5 HU vs. 27.4 HU; IQR, 24.1–31.1 HU, $p < 0.01$). The SNR (median 16.3; IQR, 12.0–22.0 vs. 13.9; IQR, 9.8–19.2 HU, $p = 0.03$) and CNR (median 25.2; IQR, 16.9–30.8 vs. 19.5; IQR, 14.5–23.7, $p < 0.01$) on SR-DLR was significantly higher than those on MBIR. The image quality score on SR-DLR was significantly higher than those on MBIR (median 4.0; IQR, 4.0–4.0 vs. 3.0; IQR, 3.0-4.0, $p < 0.01$).

In both two-volume datasets, a total of 150 major coronary branches were evaluated (Table 3), and representative cases are shown in Figs 2 and 3. Severe stenosis in the proximal section of the left anterior descending artery was more sharply delineated on SR-DLR than on MBIR, as confirmed by invasive coronary angiography. In contrast, the image quality was lower on SR-DLR images than those on MBIR in patients weighing 144 kg with a body mass index of 46 kg/m^2 even with higher SNR and CNR on SR-DLR images (Fig 4). A substantial interobserver agreement was observed on the overall image quality ($\kappa = 0.83$).

Coronary stent analysis

In 10 stents from seven patients, stent assessability was compared between SR-DLR and MBIR (Table 3, Fig 5). On SR-DLR, stent assessability was 100% (1, 5, 1, and 3 of 2.25, 2.5, 2.75, and 3.0 mm stents). On MBIR, 2.25 mm stents and 2/5 of the 2.5 mm stents cannot be assessed, and the remaining seven stents can be assessed (three stents unassessable on MBIR could be assessed on SR-DLR). All four stents with a diameter of 2.75 and 3.0 mm were assessable both on SR-DLR and MBIR. On quantitative analysis, 30 axial slices of 10 stents were evaluated. The FWHM-stent on SR-DLR was significantly thinner than on MBIR (median, 0.66 mm; IQR, 0.61–0.72 mm vs. 0.80 mm; IQR, 0.68–0.86 mm, $p < 0.01$; Fig 1e). The FWHM-lumen calculated on SR-DLR was significantly larger than on MBIR (median, 1.82 mm; IQR, 1.57–1.95 mm vs. 1.34 mm; IQR, 1.26–1.60 mm, $p < 0.01$; Fig 1f).

Discussion

To the best of our knowledge, this is the first study to evaluate the SR-DLR on the image quality of the coronary arteries and in-stent lumen. The image noise was significantly lower, and the SNR and CNR at the proximal coronary arteries was significantly higher on SR-DLR than those on MBIR images. Thus, the overall image quality was significantly better on SR-DLR images. Furthermore, stent struts were

significantly thinner, and in-stent lumens were significantly larger on SR-DLR than on MBIR in coronary stent analysis.

Development of CCTA

CCTA has become a first-line test to evaluate patients suspected of coronary artery disease. Nevertheless, some factors such as high image noise, insufficient vessel enhancement, and blooming- and beam-hardening artifacts may hamper the precise evaluation of vessel stenosis and stents [1-3]. Recent developments of UHRCT have enabled the evaluation of calcified, stented, or small diameter segments due to the greater spatial resolution [4-6]. However, radiation exposure for UHRCT was higher than that for conventional CCTA [5]. Moreover, UHRCT cannot be used in patients with higher heart rates and weight and those with arrhythmia due to the limitation of the gantry rotation time [4-6]. Remarkably, the whole heart coverage by the area detector with a faster rotation speed contributed to the improvement in the temporal resolution and decreased the radiation exposure and contrast media.

SR-DLR performance

Recently, DLR was developed to improve spatial resolution and low-contrast detectability while reducing noise due to the power of machine learning, a form of artificial intelligence [12]. Especially, SR-DLR algorithm trained using data acquired on the commercially available UHRCT system is available [7]. SR-DLR algorithm features UHR 0.25 mm detectors to maximize the inherent spatial resolution on the conventional 320-detector row CT. With conventional reconstruction, a long tradeoff between spatial resolution and noise has forced CT systems to operate at much lower spatial resolution levels than the detector and focal spots are capable of producing maintenance at clinically acceptable dose levels. With DLR, not only can this resolution be utilized, without increasing the dose or noise, but it also can be enhanced further. Furthermore, the neural network behind SR-DLR does not learn features solely in the axial plane but rather in three dimensions, indicating that signal features are identified and preserved in all three planes. Therefore, SR-DLR is found to be well-suited for cardiac exams, which are usually reviewed in CPR.

In several studies, the spatial resolution is reported be higher on MBIR than on filtered back projection and hybrid-IR images [16,17]. Reportedly, the sophisticated MBIR modeling reduces blooming artifacts and yields a better image quality than hybrid IR [18]. In this study, SR-DLR images yielded a higher image quality including image noise reduction and better spatial resolution than those on MBIR. Moreover, the reconstruction time was significantly shorter on SR-DLR than on MBIR. Hence, using SR-DLR would improve the utility of CCTA in routine clinical practice.

Assessment of the in-stent lumen on CCTA with SR-DLR

Direct visualization of the in-stent lumen on CCTA was challenging mainly due to beam hardening and partial volume effects. Motoyama *et al.* have reported that the in-stent lumen of stents with ≥2.5 mm diameter could be assessed on UHRCT because of improved spiral resolution [4]. In this study, SR-DLR

could evaluate all stents, including 2.25 and 2.5 mm stents. Moreover, SR-DLR demonstrates better strut delineation of the stent and in-stent lumen that are more accurate than MBIR. The edge has been reportedly sharper on MBIR than on images reconstructed with conventional filtered back projection or hybrid IR [18,19]. SR-DLR had similar effects on the boundary of coronary stents. Further studies are needed to compare the coronary stent evaluation between UHRCT and 320-detector row CT scanner with SR-DLR; however, SR-DLR has the potential to overcome the UHRCT limitations.

In contrast, the image quality of SR-DLR was lower in patients with higher weight. Training the deep learning neural network with educational images from higher weight patients would make the SR-DLR more valuable.

Limitations

First, our study population was small; thus, a large-scale trial is needed to confirm our preliminary results. Second, the SNR and CNR were evaluated in the proximal coronary arteries only. The small diameter of distal segments makes it impossible to place ROIs without including parts of the vessel walls and adjacent tissues. Third, the SR-DLR algorithm is currently vendor-specific. Fourth, the population of this study is less challenging for CCTA scans. Further studies are needed to prove the value of SR-DLR in patients with higher calcium score and weight and those with arrhythmia. Finally, the diagnostic accuracy of CCTA was confirmed in comparison with invasive coronary angiography in a limited number of enrolled patients only. Further studies are needed to evaluate the diagnostic accuracy of the SR-DLR using invasive coronary angiography as the reference standard.

Conclusion

SR-DLR improves the image quality of the coronary arteries and in-stent lumen at CCTA. Datasets reconstructed with SR-DLR empower the clinician with the high-contrast signal definition and reduce noise, relative to conventional MBIR.

Abbreviations

CCTA, coronary computed tomography angiography; SR-DLR, super-resolution deep learning reconstruction; MBIR, model-based iterative reconstruction; UHRCT, ultrahigh spatial resolution computed tomography; ECG, electrocardiogram; SD, standard deviation; ROI, region of interest; SNR, signal-to-noise ratio; CNR, contrast-to-noise ratio; CPR, curved planar reformation; FWHM-lumen, full width at half maximum of the lumen; FWHM-stent, full width at half maximum of the stent; IQR, interquartile range

Declarations

Funding sources: None

Conflicts of interest: Kunihiro Yoshioka received a research grant from Canon Medical Systems Co. Ltd. Other authors declare that they have no conflict of interest.

Authors' contributions: MO designed and drafted the manuscript. MO and KY acquired data and assessed CCTA. MS and TO supported the statistical analysis. YU, TC, and TS provided technical assistance. KY substantially contributed to the manuscript and revised it critically for important intellectual content. All authors approved the submitted version.

Unblinded Acknowledgments: The authors would like to thank Enago (www.enago.jp) for the English language review.

Date sharing statement: The dataset analyzed during the present study is available from the corresponding author on reasonable request.

Ethics approval: The study was approved by the institution's human research committee (Iwate Medical University).

Consent to participate:

Informed consent was obtained from all individual participants included in the study.

References

1. Raff GL, Gallagher MJ, O'Neill WW, Goldstein JA (2005) Diagnostic accuracy of noninvasive coronary angiography using 64-slice spiral computed tomography. J Am Coll Cardiol 46:552–557. doi: 10.1016/j.jacc.2005.05.056
2. Nikolaou K, Knez A, Rist C, Wintersperger BJ, Leber A, Johnson T, Reiser MF, Becker CR (2006) Accuracy of 64-MDCT in the diagnosis of ischemic heart disease. AJR Am J Roentgenol 187:111–117. doi: 10.2214/AJR.05.1697
3. Herzog C, Zwerner PL, Doll JR, Nielsen CD, Nguyen SA, Savino G, Vogl TJ, Costello P, Schoepf UJ (2007) Significant coronary artery stenosis: comparison on per-patient and per-vessel or per-segment basis at 64-section CT angiography. Radiology 244:112–120. doi: 10.1148/radiol.2441060332
4. Motoyama S, Ito H, Sarai M, Nagahara Y, Miyajima K, Matsumoto R, Doi Y, Kataoka Y, Takahashi H, Ozaki Y, Toyama H, Katada K (2018) Ultra-high-resolution computed tomography angiography for assessment of coronary artery stenosis. Circ J 82:1844–1851. doi: 10.1253/circj.CJ-17-1281
5. Takagi H, Tanaka R, Nagata K, Ninomiya R, Arakita K, Schuijf JD, Yoshioka K (2018) Diagnostic performance of coronary CT angiography with ultra-high-resolution CT: comparison with invasive coronary angiography. Eur J Radiol 101:30–37. doi: 10.1016/j.ejrad.2018.01.030
6. Latina J, Shabani M, Kapoor K, Whelton SP, Trost JC, Sesso J, Demehri S, Mahesh M, Lima JAC, Arbab-Zadeh A (2021) Ultra-high-resolution coronary CT angiography for assessment of patients

with severe coronary artery calcification: initial experience. Radiol Cardiothorac Imaging 3:e210053. doi: 10.1148/ryct.2021210053

7. Hernandez AM, Shin DW, Abbey CK, Seibert JA, Akino N, Goto T, Vaishnav JY, Boedeker KL, Boone JM (2020) Validation of synthesized normal-resolution image data generated from high-resolution acquisitions on a commercial CT scanner. Med Phys 47:4775–4785. doi: 10.1002/mp.14395
8. Abbara S, Arbab-Zadeh A, Callister TQ, Desai MY, Mamuya W, Thomson L, Weigold WG (2009) SCCT guidelines for performance of coronary computed tomographic angiography: a report of the Society of Cardiovascular Computed Tomography Guidelines Committee. J Cardiovasc Comput Tomogr 3:190–204. doi: 10.1016/j.jcct.2009.03.004
9. Abbara S, Blanke P, Maroules CD, Cheezum M, Choi AD, Han BK, Marwan M, Naoum C, Norgaard BL, Rubinshtein R, Schoenhagen P, Villines T, Leipsic J (2016) SCCT guidelines for the performance and acquisition of coronary computed tomographic angiography: a report of the society of cardiovascular Computed Tomography Guidelines Committee: endorsed by the North American Society for Cardiovascular Imaging (NASCI). J Cardiovasc Comput Tomogr 10:435–449. doi: 10.1016/j.jcct.2016.10.002
10. The 2007 recommendations of the International Commission on Radiological Protection (2007) Ann ICRP ICRP Publication 37:1–332. doi: 10.1016/j.icrp.2007.10.003. ICRP publication 103
11. Leipsic J, Abbara S, Achenbach S, Cury R, Earls JP, Mancini GJ, Nieman K, Pontone G, Raff GL (2014) SCCT guidelines for the interpretation and reporting of coronary CT angiography: a report of the Society of Cardiovascular Computed Tomography Guidelines Committee. J Cardiovasc Comput Tomogr 8:342–358. doi: 10.1016/j.jcct.2014.07.003
12. Tatsugami F, Higaki T, Nakamura Y, Yu Z, Zhou J, Lu Y, Fujioka C, Kitagawa T, Kihara Y, Iida M, Awai K (2019) Deep learning-based image restoration algorithm for coronary CT angiography. Eur Radiol 29:5322–5329. doi: 10.1007/s00330-019-06183-y
13. Lembcke A, Wiese TH, Schnorr J, Wagner S, Mews J, Kroencke TJ, Enzweiler CN, Hamm B, Taupitz M (2004) Image quality of noninvasive coronary angiography using multislice spiral computed tomography and electron-beam computed tomography: intraindividual comparison in an animal model. Invest Radiol 39:357–364. doi: 10.1097/01.rli.0000123316.10765.6c
14. Tatsugami F, Husmann L, Herzog BA, Burkhard N, Valenta I, Gaemperli O, Kaufmann PA (2009) Evaluation of a body mass index-adapted protocol for low-dose 64-MDCT coronary angiography with prospective ECG triggering. AJR Am J Roentgenol 192:635–638. doi: 10.2214/AJR.08.1390
15. Groen JM, Greuter MJ, van Ooijen PM, Oudkerk M (2007) A new approach to the assessment of lumen visibility of coronary artery stent at various heart rates using 64-slice MDCT. Eur Radiol 17:1879–1884. doi: 10.1007/s00330-006-0568-8
16. Nelson RC, Feuerlein S, Boll DT (2011) New iterative reconstruction techniques for cardiovascular computed tomography: how do they work, and what are the advantages and disadvantages? J Cardiovasc Comput Tomogr 5:286–292. doi: 10.1016/j.jcct.2011.07.001

17. Geyer LL, Schoepf UJ, Meinel FG, Nance JW Jr, Bastarrika G, Leipsic JA, Paul NS, Rengo M, Laghi A, De Cecco CN (2015) State of the art: iterative CT reconstruction techniques. Radiology 276:339–357. doi: 10.1148/radiol.2015132766
18. Tatsugami F, Higaki T, Sakane H, Fukumoto W, Kaichi Y, Iida M, Baba Y, Kiguchi M, Kihara Y, Tsushima S, Awai K (2017) Coronary artery stent evaluation with model-based iterative reconstruction at coronary CT angiography. Acad Radiol 24:975–981. doi: 10.1016/j.acra.2016.12.020
19. Yokomachi K, Tatsugami F, Higaki T, Kume S, Sakamoto S, Okazaki T, Kurisu K, Nakamura Y, Baba Y, Iida M, Awai K (2019) Neointimal formation after carotid artery stenting: phantom and clinical evaluation of model-based iterative reconstruction (MBIR). Eur Radiol 29:161–167. doi: 10.1007/s00330-018-5598-5

Tables

Table 1. Baseline characteristics

Patient demographics (n = 50)	
Age, years	68 (59–74)
Male patients, n (%)	34 (68)
Height, cm	168 (158–171)
Weight, kg	65 (55–74)
Body surface area, m^2	1.7 (1.6–1.9)
Body mass index, kg/m^2	24 (22–26)
Hypertension, n (%)	35 (70)
Dyslipidemia, n (%)	28 (56)
Diabetes, n (%)	15 (30)
Smoking history (former or current), n (%)	13 (26)
Sinus rhythm, n (%)	46 (92)
Characteristics of CCTA scanning	
Mean heart rate during CCTA scanning, bpm	56 (51–63)
Tube voltage 100/120 kV, n (%)	23 (46)/27 (54)
Tube current	
With 100 kV, mA	315 (250–368)
With 120 kV, mA	400 (235–595)
Total dose length product, mGy*cm	56 (44–117)
Total effective radiation dose, mSv	0.7 (0.6–1.6)
Contrast medium dose, mL	48 (42–58)
Calcium score	3 (0–127)

CCTA, coronary computed tomography angiography

Table 2. Comparison of reconstruction time, image noise, signal-to-noise ratio, contrast-to-noise ratio, and visual evaluation of coronary arteries between super-resolution deep learning reconstruction and model-based iterative reconstruction

Parameter	SR-DLR	MBIR	p-value
Reconstruction time, s	97 (88–103)	172 (161–185)	< 0.01
Image noise, HU			
Ascending aorta	22.4 (19.4–29.9)	28.8 (25.6–36.5)	< 0.01
Left atrium	22.4 ± 3.9	30.1 ± 5.1	< 0.01
Septal wall of the ventricle	20.5 ± 3.8	23.5 ± 3.8	< 0.01
All locations	22.1 (19.1–24.5)	27.4 (24.1–31.1)	< 0.01
SNR	16.3 (12.0–22.0)	13.9 (9.8–19.2)	0.03
CNR	25.2 (16.9–30.8)	19.5 (14.5–23.7)	< 0.01
Overall quality (scale 1–4)	4.0 (4.0–4.0)	3.0 (3.0–4.0)	< 0.01

SR-DLR, super-resolution deep learning reconstruction; MBIR, model-based iterative reconstruction; SNR, signal-to-noise ratio; CNR, contrast-to-noise ratio

Table 3. Characteristics of coronary artery stenosis and stent

Stenosis assessment (n = 150)	
<25%, n (%)	57 (38)
25–49%, n (%)	62 (41)
50–69%, n (%)	21 (14)
70–99%, n (%)	10 (7)
Stent diameter (n = 10)	
2.25 mm, n (%)	1 (10)
2.5 mm, n (%)	5 (50)
2.75 mm, n (%)	1 (10)
3.0 mm, n (%)	3 (30)
Stent length (n = 10)	30 ± 10
Stent lesion (n = 10)	
Right coronary artery, n (%)	0 (0)
Left anterior descending artery, n (%)	7 (70)
Left circumflex artery, n (%)	3 (30)

Figures

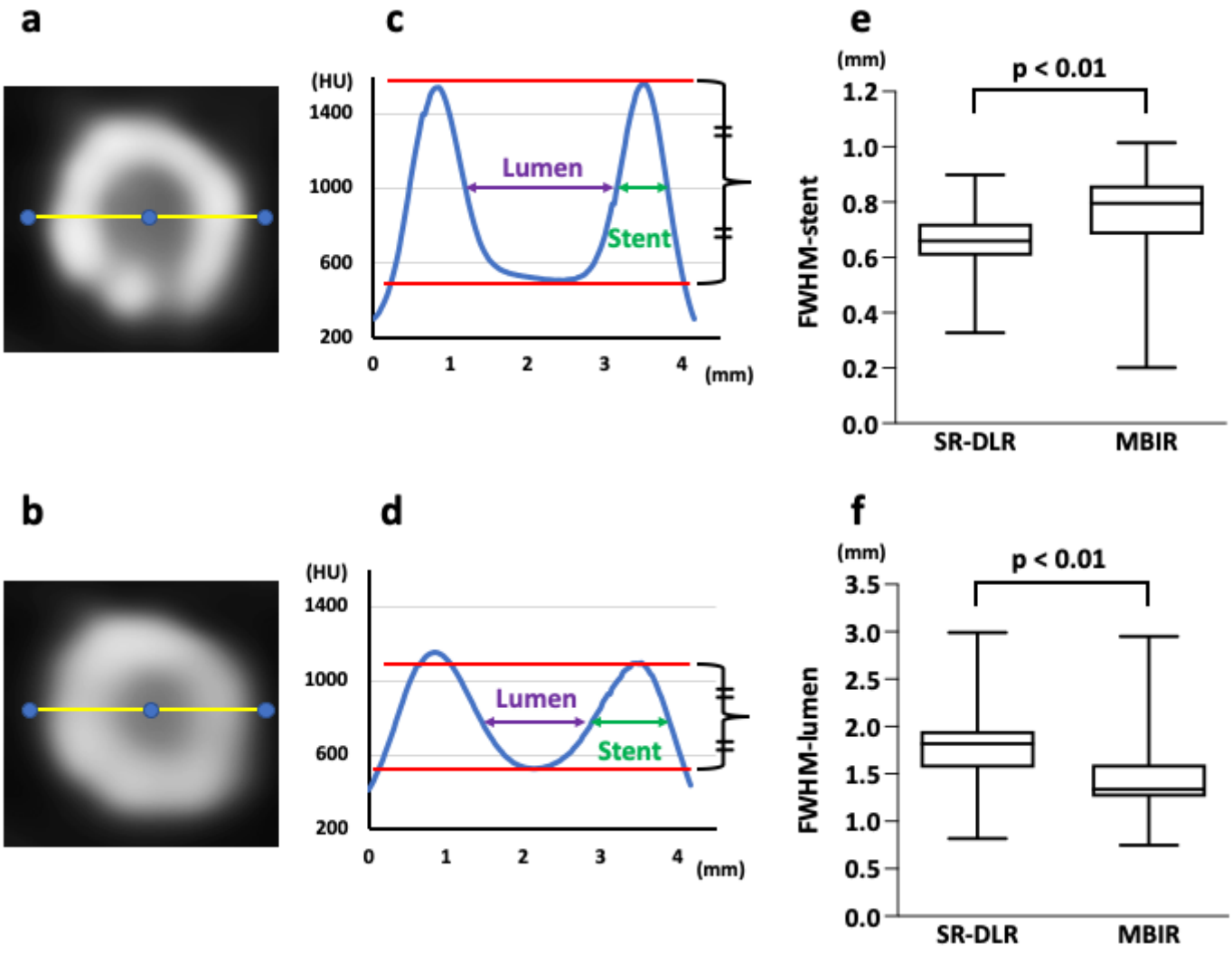

Figure 1

Title: Quantitative analysis of the lumen and stent in the coronary artery.

After identifying the center of the stent on a cross-sectional image, attenuation profiles were calculated (a: SR-DLR, b: MBIR). FWHM-lumen and FWHM-stent were measured (c: SR-DLR, d: MBIR). FWHM-stent was significantly thinner ($p < 0.01$), whereas FWHM-lumen was significantly larger on SR-DLR ($p < 0.01$) than on MBIR (e, f). SR-DLR, super-resolution deep learning reconstruction; MBIR, model-based iterative reconstruction; FWHM-lumen, full width at half maximum of the lumen; FWHM-stent, full width at half maximum of the stent

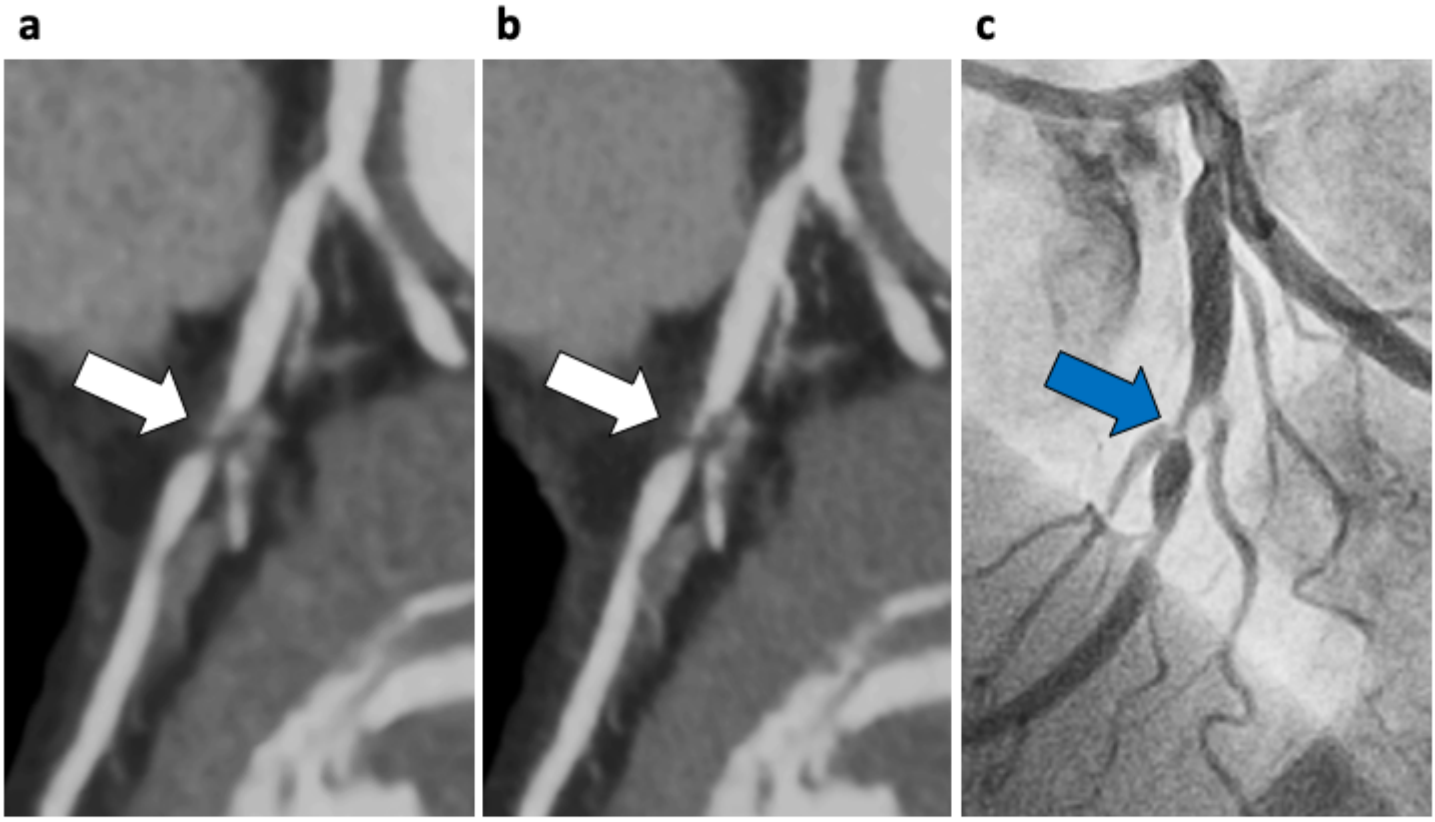

Figure 2

Title: Case example of a 66-year-old woman with effort angina.

Curved planar reformation of the left anterior descending artery (LAD) on MBIR (a) and SR-DLR (b). Severe stenosis in the proximal section of the LAD was more sharply delineated on SR-DLR than those on MBIR (white arrows), which was confirmed using invasive coronary angiography (c, blue arrow). SR-DLR, super-resolution deep learning reconstruction; MBIR, model-based iterative reconstruction; LAD, left anterior descending artery

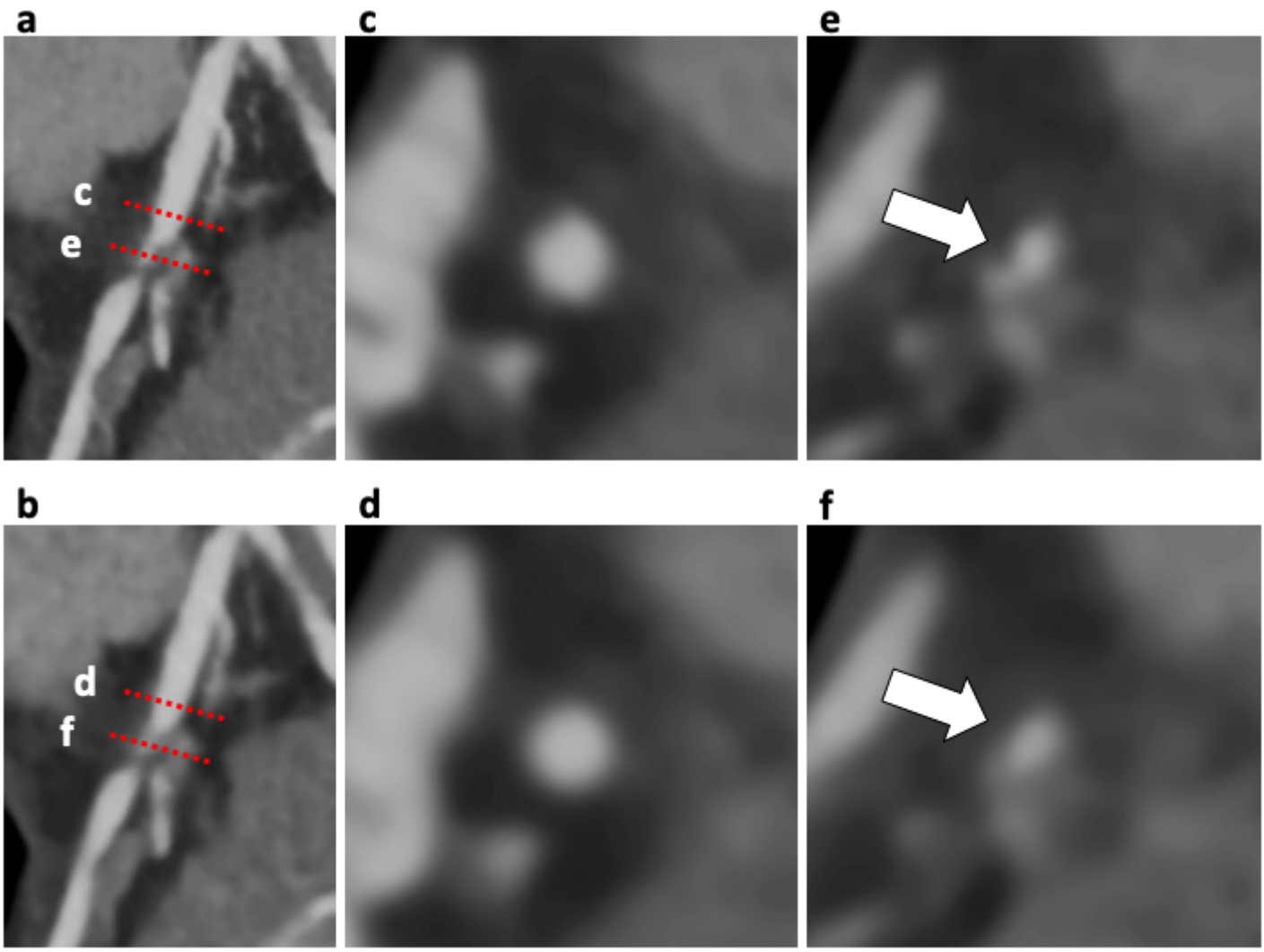

Figure 3

Title: Case example of the patient in Fig 2.

Curved planar reformation (CPR) images in the proximal section of the left anterior descending artery (LAD) with SR-DLR (a) and MBIR (b). Two cross-sectional images show the proximal reference site (c and d) and the site of maximal stenosis (e and f) correspond to red dashed lines on the CPR image. Coronary lumen and plaque (white arrows) were more sharply delineated on SR-DLR (c, e) than those on MBIR (d, f). CPR, curved planar reformation; LAD, left anterior descending artery; SR-DLR, super-resolution deep learning reconstruction; MBIR, model-based iterative reconstruction

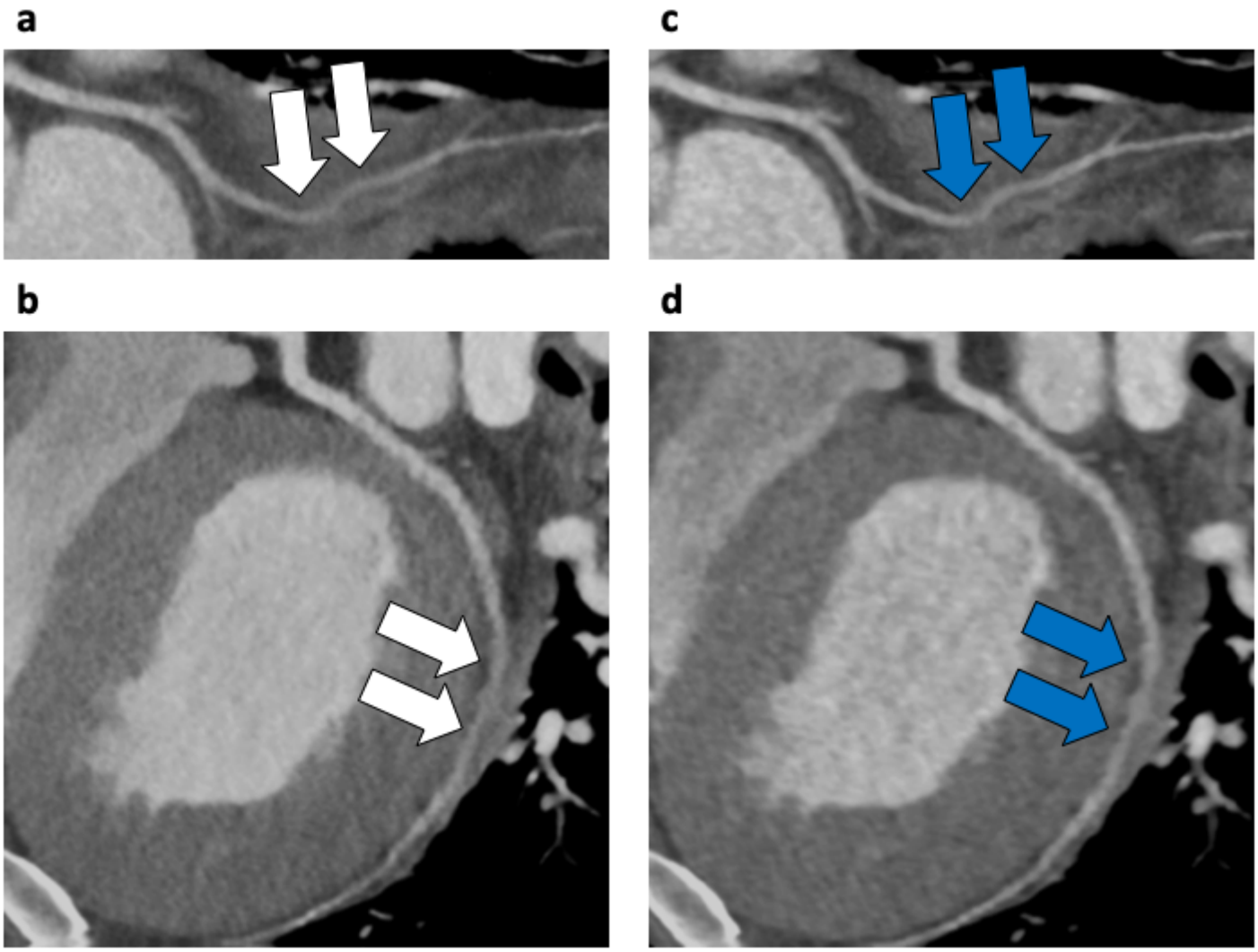

Figure 4

Title: Case example of a 34-year-old man weighing 144 kg with a body mass index of 46 kg/m^2.

Curved planar reformation of the left circumflex artery taken at 120 kV, 750 mA, with prospective ECG gating. a, b: SR-DLR image (signal-to-noise ratio (SNR), 17.4; contrast-to-noise ratio (CNR), 21.0). The image quality was rated as fair with marked noise-related blurring (white arrows). c, d: MBIR image (SNR, 16.0; CNR, 17.8). The image quality was rated as good with some noise-related blurring (blue arrows). SR-DLR, super-resolution deep learning reconstruction; SNR, signal-to-noise ratio; CNR, contrast-to-noise ratio; MBIR, model-based iterative reconstruction

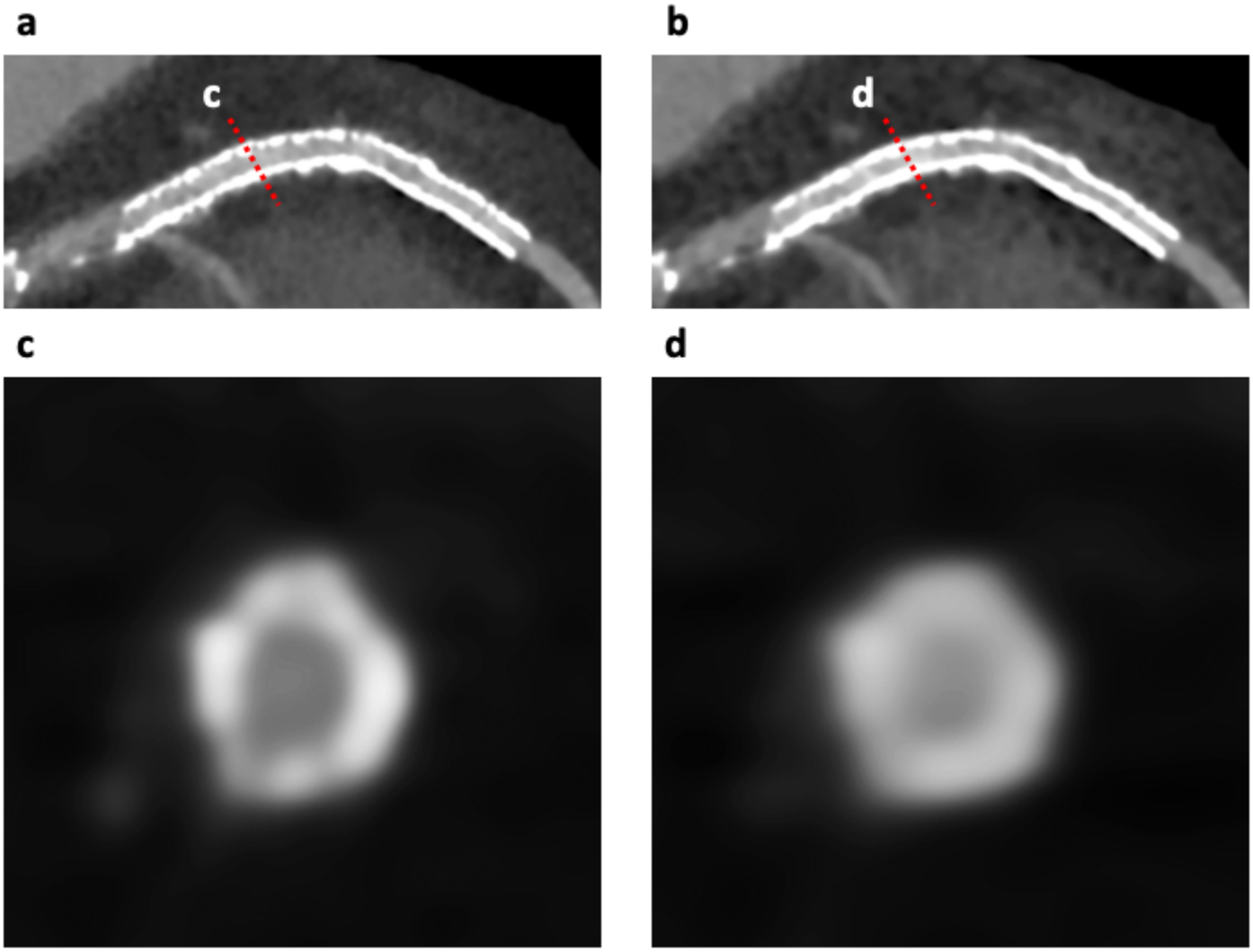

Figure 5

Title: Case example of an 80-year-old woman with a stent in the left descending coronary artery.

Curved planar reformation (CPR) images of the 2.5 mm stent in the left anterior descending artery (LAD) with SR-DLR (a) and MBIR images (b). Cross-sectional images showing the in-stent lumen and stent strut (c and d) corresponding to red dashed lines on the CPR image. In-stent lumen was clearly visualized on SR-DLR (a and c; assessable) compared with MBIR (b and d; unassessable). CPR, curved planar reformation; LAD, left anterior descending artery; SR-DLR, super-resolution deep learning reconstruction; MBIR, model-based iterative reconstruction